Phytochemistry 205 (2023) 113480

Contents lists available at ScienceDirect

Phytochemistry

journal homepage: www.elsevier.com/locate/phytochem

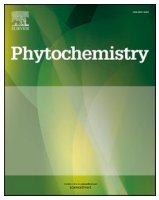

Pholiols E–K, lanostane-type triterpenes from *Pholiota populnea* with anti-inflammatory properties

Morteza Yazdani [a], Anita Barta [a], Róbert Berkecz [b], Orinamhe Godwin Agbadua [a], Attila Ványolós [c], Judit Hohmann [a,d,e,*]

[a] Institute of Pharmacognosy, University of Szeged, Eötvös u. 6, H-6720, Szeged, Hungary
[b] Institute of Pharmaceutical Analysis, University of Szeged, Somogyi u. 4, 6720, Szeged, Hungary
[c] Department of Pharmacognosy, Semmelweis University, Üllői u. 26, H-1085, Budapest, Hungary
[d] Interdisciplinary Centre for Natural Products, University of Szeged, Eötvös u. 6, H-6720, Szeged, Hungary
[e] ELKH-USZ Biologically Active Natural Products Research Group, University of Szeged, Eötvös u. 6, H-6720, Szeged, Hungary

ARTICLE INFO

Keywords:
Pholiota populnea
Strophariaceae
Anti-inflammatory activity
Lanostane triterpenes
Pholiols e–k

ABSTRACT

Investigation of the chloroform and ethyl acetate extracts of the edible mushroom *Pholiota populnea* led to the isolation of eight triterpenes, the undescribed natural products pholiols E–K and the known (+)-clavaric acid. HRESIMS and 1D and 2D NMR spectroscopy were employed to determine the structures of the undescribed compounds. The NOESY spectra were used to assign the relative configurations of triterpenes. The isolated compounds were screened for their anti-inflammatory activity on cyclooxygenase (COX-1 and COX-2), and lipoxygenase (5-LOX and 15-LOX) inhibitory assays. Dose–response investigations revealed that lanostane derivatives exhibited moderate 5-LOX and COX-2 inhibitory activities, with pholiol F (IC_{50} 194.5 μM against 5-LOX and 439.8 μM against COX-2) the most active among the isolated compounds. Our findings indicated that *P. populnea* is an abundant source of new bioactive lanostane-type triterpenes.

1. Introduction

The nutritional, medicinal, and bioremediation significance of mushrooms has recently increased because they are an abundant source of nutrients and bioactive compounds, including polysaccharides, proteins, fats, phenolics, alkaloids, terpenoids, nucleosides, lectins, minerals, and vitamins. Triterpenoids and steroids frequently occur among the fungal metabolites that can be classified into nine primary groups based on their carbon skeletons: squalene, lanostane, ergostane, fernane, friedelane, lupane, malabaricane, eburicane, and cucurbitane (Öztürk et al., 2015). The most frequently occurring triterpenes are lanostane and ergostane; other triterpenoids are relatively uncommon mushroom metabolites. Generally, the compounds are substituted with hydroxy, keto, aldehyde, and carboxyl groups or have ether and acetonide functionalities. Esterification is also a characteristic of some fungal triterpenes; esterifying acids are simple organic or fatty acids. Some compounds have special structures, including lactones, seco-ring-A, or nor-triterpenoids. Several compounds were also found to have potent bioactivities, such as cytotoxic, anti-invasive, anti-inflammatory, antimycobacterial, anticandidal, antimalarial, antiviral, and anticholinesterase, and effects on adipocyte differentiation (Öztürk et al., 2015).

In the literature, numerous examples can be found where fungal triterpenes are efficient in anti-inflammatory test models. Lanostane triterpenes of *Macrolepiota procera*, called lepiotaprocerins, were found to inhibit nitric oxide (NO) production (Chen et al., 2018). *Ganoderma lucidum*, which is extensively used in traditional Chinese medicine, was investigated for its protective effect on lipopolysaccharide-induced inflammatory responses and acute liver injury. Triterpenes were also found to play a crucial role in the inhibition of inflammatory diseases by blocking nuclear factor κ-activated B cell (NF-κB) and mitogen-activated protein kinase (MAPK) signaling pathways (Hu et al., 2020). The edible cultivated mushroom *Wolfiporia cocos* is also abundant in lanostane triterpenes; its constituent, poricoic acid GM, was also found to inhibit NO production (IC_{50} 9.73 μM), inducible nitric oxide synthase (iNOS), and cyclooxygenase-2 (COX-2) protein expression in LPS-induced RAW264.7 murine macrophages (Bao et al., 2019). Lanostane triterpenoids and ergosterols isolated from the fruiting bodies of *Pyropolyporus fomentarius* also exhibited inhibitory activities against NO production in the same test model (Zhang et al., 2021). Triterpenes of *Hypholoma*

* Corresponding author. Institute of Pharmacognosy, University of Szeged, Eötvös u. 6, H-6720, Szeged, Hungary.
E-mail address: hohmann.judit@szte.hu (J. Hohmann).

https://doi.org/10.1016/j.phytochem.2022.113480
Received 25 July 2022; Received in revised form 30 September 2022; Accepted 16 October 2022
Available online 22 October 2022

lateritium exerted a significant inhibitory effect on COX-2 and were able to promote the Nrf2 pathway. Fasciculol C, the hexahydroxylated lanostane, synthesized the highest level of Nrf2 (Ványolós et al., 2020).

The present study focused on the isolation, structural determination, and biological activity evaluation of the compounds of *Pholiota populnea* (Pers.) Kuyper & Tjall.-Beuk. [syn. *Pholiota destruens* (Brond.) Quel., *Hemipholiota populnea* (Pers.) Kühner ex Bon] (Strophariaceae) as a continuation of our study on bioactive fungal metabolites. This mushroom is not poisonous and is robust with a large cap and white to buff scales. In our previous study, four undescribed lanostane diesters, called pholiols A–D were reported, together with an acyclic triterpene tetraol, ergosterol, and 3β-hydroxyergosta-7,22-diene from the *n*-hexane extract of *P. populnea* (Yazdani et al., 2022). These isolates were investigated for their cytotoxic activity against human colon adenocarcinoma cells (Colo205 and Colo320). The combination with doxorubicin and the efflux pump inhibitory activity of the compounds on drug-resistant Colo 320 cells was also assayed, and the P-glycoprotein efflux pump modulatory effects and synergism of triterpenes with doxorubicin were discovered.

Investigation of the chloroform and ethyl acetate extracts of *P. populnea* led to the isolation of seven undescribed triterpenes, namely, pholiols E–K (**1–7**), and the known (+)-clavaric acid (**8**) (Fig. 1). On cyclooxygenase (COX-1, COX-2) and lipoxygenase (5-LOX and 15-LOX) assays, the anti-inflammatory activity of the isolated compounds (**1–8**) and the previously isolated pholiol C (**9**) (Yazdani et al., 2022) was evaluated.

2. Results and discussion

2.1. Structure elucidation of triterpenes (1–8)

Compound **1** was isolated as a white amorphous powder with an optical rotation of $[\alpha]_D^{25}$ +49 (*c* 0.1, MeOH). Its protonated molecular ion at *m/z* 617.4063 $[M+H]^+$ (calcd for $C_{36}H_{57}O_8$ 617.4048) in the HRESIMS spectrum offered the molecular formula $C_{36}H_{56}O_8$. The ^{1}H NMR spectrum exhibited the presence of a 3-hydroxy-3-methylglutarate [δ_H

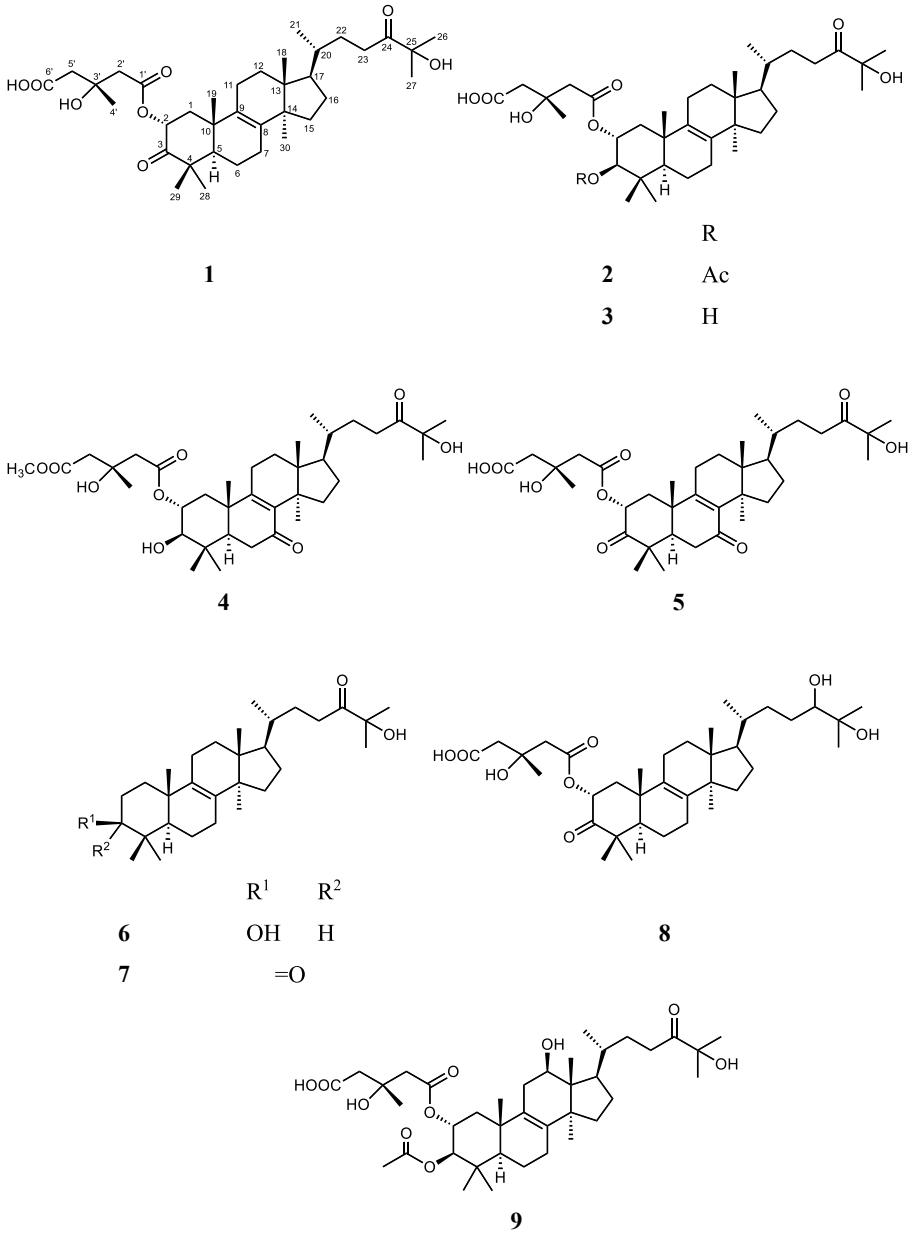

Fig. 1. Compounds **1–9** isolated from *Pholiota populnea*.

2.80 m (2H), 2.75 m (2H), 1.41 s (CH_3); δ_C 2 × 171.63, 2 × 46.56, 45.83, 70.90, 27.56] ester group in the molecule characteristic to members of pholiol series (Yazdani et al., 2022) (Tables 1 and 2). Furthermore, the ^{1}H NMR spectrum demonstrated resonances of seven tertiary (δ_H 1.40, 2 × 1.30, 1.11, 1.18, 0.93, and 0.78, each 3H, s) and one secondary (δ_H 0.94, 3H, d, J = 6.2 Hz) methyl groups as well as one oxymethine (δ_H 5.67, dd, J = 13.62 and 5.6 Hz). From the ^{13}C J-MOD spectrum, two keto groups (δ_C 210.92 and 217.79) and an oxygen-substituted non-protonated carbon (δ_C 77.90) could be identified. The presence of a tetrasubstituted olefin bond was obvious from the nonprotonated sp^2 carbon signals at δ_C 136.90 and 134.69. The 1D NMR data proposed that compound **1** is a lanostanol-en-dione monoester. Regarding its HMBC correlations with δ_H 2.36 (H-1a), 1.66 (H-1b), 5.67 (H-2), 1.11 (H_3-28), and 1.18 (H_3-29), the keto group at δ_C 210.92 was placed at C-3. The other keto group (δ_C 217.79) was concluded to be at C-24 based on its long-range correlations with δ_H 1.30 (H_3-26, H_3-27) and 2.67 (H_2-23). The HMBC correlations of C-25 (δ_C 77.90) with protons at δ_H 1.30 (H_3-26 and H_3-27) depicted the hydroxy group at C-25, whereas correlations between δ_C 171.63 (C-1′) and δ_H 5.67 (H-2) as well as 2.80 and 2.75 (H_2-2') were indicative of the position of the ester group at C-2. Based on the HMBC cross-peaks of signals at δ_C 136.90 (C-8) with δ_H 0.93 (H_3-30), 2.18 (H_2-7), and 1.73 (H-6) as well as δ_C 134.69 (C-9) with δ_H 1.40 (H_3-19) and 2.18 (H_2-7), the location of the olefin group at C-8–C-9 was determined. The relative configuration of compound **1** was examined using diagnostic Overhauser effects detected in a NOESY spectrum. The NOESY correlations of H-2 (δ_H 5.67) with H_3-19 (δ_H 1.40), H_3-29 (δ_H 1.18), and H-1a (δ_H 2.36) pointed these protons in the β orientation and the ester group in the α orientation. The NOEs between H_3-18/H-20 and H-17/H_3-30 were in line with those of lanostane triterpenes (Aichour et al., 2014). The above findings were consistent with the proposed structure of compound **1** [2α-(3-hydroxy-3-methylglutaroyloxy)-25-hydroxylanosta-8-en-3,24-dione], which was called pholiol E (**1**) (Fig. 1).

Compound **2** was obtained as a white amorphous powder with $\alpha]_D^{25}$ +5 (c 0.1, $CHCl_3$). Its molecular formula was deduced to be $C_{38}H_{60}O_9$ from the protonated molecular ion at m/z 661.4320 $[M+H]^+$ (calcd for $C_{38}H_{61}O_9$, 661.4310) detected in the HRESIMS spectrum. A comprehensive analysis of ^{1}H and ^{13}C J-MOD as well as 2D data demonstrated the presence of the same parent system and 3-hydroxy-3-methylglutarate moiety as in compound **1**, except the C-3 keto group, which was replaced by an acetoxy group (Tables 1 and 2). The acetoxy group is attached at C-3, as demonstrated by the sequences of the correlated protons in the ^{1}H–^{1}H–COSY spectrum: CH_2–CH(OR)–CH(OR)–(δ_H 2.11 m, 1.38 m, 5.19 t (10.8 Hz), 4.79 d). The location of the ester functionalities was corroborated by the HMBC correlations observed between δ_C 171.14 (C-1′) and δ_H 5.19 (H-2), 2.62 and 2.51 (H-2') and δ_C 171.84 (AcCO) and δ_H 4.79 (H-3), and 2.10 (AcMe), showing 3-hydroxy-3-methylglutarate at C-2 and acetate at C-3. The coupling constant of H-2 and H-3 (J = 10.5 Hz) and NOESY correlations between H-3 (δ_H 4.79)/H-1b (δ_H 1.38), H-3/H_3-28 (δ_H 0.92), H-2 (δ_H 5.19)/H-1a (δ_H 2.11), and H-2/H_3-29 (δ_H 0.95) confirmed the opposite orientation of the ester groups. The Overhauser effect of H-2 with H_3-19 (δ_H 1.13) indicated the H-2β and H-3α positions. Thus, the structure of this compound was elucidated as 2α-(3-hydroxy-3-methylglutaroyloxy)-3-acetoxy-25-hydroxylanosta-8-en-24-one (**2**), called pholiol F.

Table 1
^{1}H NMR data of compounds **1**–**8** (500 MHz, δ ppm, J = Hz).

H	1[a]	2[b]	3[a]	4[a]	5[a]	6[a]	7[b]	8[a]
1	2.36 dd (12.3, 5.6), 1.66 m	2.11 m, 1.38 m	2.05 m, 1.18 m	2.20 dd (12.3, 4.3), 1.45 m	2.50 m, 1.93 t (13.1)	1.76 m, 1.22 m	1.98 m, 1.61 m	2.36 dd (12.3, 5.6), 1.66 m
2	5.67 dd (13.6, 5.6)	5.19 dt (3.4, 10.5)	4.92 dt (3.9, 10.6)	5.07 dt (4.3, 11.5)	5.72 dd (13.5, 5.8)	1.63 m (2H)	2.57 m, 2.41 ddd (15.8, 6.7, 3.5)	5.66 dd (13.4, 5.6)
3	–	4.79 d (10.5)	3.20 d (10.1)	3.24 d (10.1)	–	3.17 dd (10.1, 6.3)	–	–
5	1.53 m	1.51 m	1.53 m	1.77 m	2.10 dd (14.6, 3.2)	1.06 m	1.60 m	1.53 m
6	1.80 m, 1.73 m	1.69 m, 1.56 m	1.74 m, 1.57 m	2.55 dd (16.3, 14.5), 2.36 m	2.73 m, 2.32 dd (16.6, 3.2)	1.71 m, 1.54 m	1.61 m (2H)	1.80 m, 1.72 m
7	2.18 m (2H)	2.09 m (2H)	2.10 m (2H)	–	–	2.07 m (2H)	2.08 m (2H)	2.17 m (2H)
11	2.16 m, 2.09 m	2.00 m (2H)	2.04 m (2H)	2.38 m (2H)	2.47 m (2H)	2.06 m (2H)	2.04 m (2H)	2.16 m, 2.10 m
12	1.79 m (2H)	1.73 m (2H)	1.74 m (2H)	1.84 m (2H)	1.87 m (2H)	1.78 m, 1.72 m	1.75 m, 1.70 m	1.81 m (2H)
15	1.78 m, 1.23 m	1.61 m, 1.21 m	1.65 m, 1.22 m	2.01 m, 1.72 m	2.03 m, 1.76 m	1.67 m, 1.21 m	1.62 m, 1.22 dd (13.7, 2.5)	1.69 m, 1.25 m
16	2.01 m, 1.46 m	1.97 m, 1.39 m	1.98 m, 1.41 m	2.00 m, 1.42 m	2.02 m, 1.45 m	1.98 m, 1.42 m	1.97 m, 1.38 m	2.01 m, 1.43 m
17	1.56 m	1.30 m	1.53 m	1.47 m	1.49 m	1.53 m	1.50 m	1.57 m
18	0.78 s	0.70 s	0.74 s	0.71 s	0.74 s	0.74 s	0.72 s	0.79 s
19	1.40 s	1.13 s	1.12 s	1.32 s	1.57 s	1.01 s	1.12 s	1.40 s
20	1.45 m	1.40 m	1.42 m	1.42 m	1.44 m	1.43 m	1.40 m	1.46 m
21	0.94 d (6.2)	0.89 d (6.4)	0.92 d (6.4)	0.95 d (6.1)	0.96 d (6.2)	0.93 d (6.2)	0.91 d (6.4)	0.96 d (6.4)
22	1.70 m, 1.27 m	1.82 m, 1.30 m	1.76 m, 1.21 m	1.77 m, 1.23 m	1.78 m, 1.30 m	1.77 m, 1.22 m	1.81 m, 1.31 m	1.82 m, 1.01 m
23	2.67 m (2H)	2.54 m, 2.50 m	2.66 m (2H)	2.66 m (2H)	2.69 m (2H)	2.65 m (2H)	2.55 m, 2.48 m	1.74 m, 1.14 m
24	–	–	–	–	–	–	–	3.17 d (9.9)
26	1.30 s	1.39 s	1.29 s	1.29 s	1.29 s	1.29 s	1.39 s	1.16 s
27	1.30 s	1.39 s	1.29 s	1.29 s	1.29 s	1.29 s	1.38 s	1.16 s
28	1.11 s	0.92 s	1.06 s	1.05 s	1.09 s	0.98 s	1.10 s	1.10 s
29	1.18 s	0.95 s	0.89 s	0.96 s	1.24 s	0.81 s	1.07 s	1.18 s
30	0.93 s	0.89 s	0.93 s	0.95 s	0.94 s	0.92 s	0.90 s	0.93 s
2′	2.80 m, 2.75 m	2.62 m, 2.51 m	2.51 m, 2.33 m	2.71 m (2H)	2.70 m, 2.65 m			2.75 m, 2.71 m
4′	1.41 s	1.39 s	1.33 s	1.41 s	1.37 s			1.41 s
5′	2.69 m (2H)	2.62 m, 2.51 m	2.66 m, 2.50 m	2.71 s (2H)	2.70 m, 2.65 m			2.75 m, 2.71 m
7′	–			3.68 s				
OAc	–	2.10 s						

[a] Recorded in CD_3OD.
[b] Recorded in $CDCl_3$.

Table 2
^{13}C NMR data of compounds **1**–**8** in CD_3OD (125 MHz, δ ppm).

Atom	1[a]	2[b]	3[a]	4[a]	5[a]	6[a]	7[b]	8[a]
1	43.68	41.28	42.21	41.10	42.36	37.01	36.22	43.69
2	73.73	71.92	74.64	73.41	72.97	28.54	34.76	73.91
3	210.92	80.47	80.59	79.99	208.51	79.72	215.13	210.87
4	49.00	39.57	40.58	40.75	49.10	39.97	47.55	49.13
5	53.97	50.58	51.78	51.15	52.57	52.04	51.40	53.99
6	19.98	18.24	19.36	37.48	37.73	19.45	19.60	19.99
7	27.21	26.39	27.42	201.26	200.27	27.69	26.50	27.22
8	136.90	135.25	136.07	139.95	140.18	135.76	135.44	136.86
9	134.69	133.50	135.21	167.19	166.56	136.09	133.35	134.76
10	39.14	38.36	39.40	42.10	41.75	38.26	37.06	39.14
11	22.56	21.40	22.19	24.89	25.34	22.08	21.23	22.51
12	32.16	31.01	32.17	31.23	31.23	32.36	31.03	32.19
13	51.05	44.77	51.05	49.07	46.23	45.80	44.70	51.04
14	45.83	50.05	45.73	46.11	49.72	51.08	50.11	45.78
15	31.11	30.90	31.84	33.18	33.17	31.92	31.12	31.81
16	29.05	28.23	29.07	41.10	29.57	29.07	28.25	29.17
17	51.82	50.26	51.78	50.36	50.30	51.86	50.56	51.94
18	16.35	15.97	16.32	16.35	16.38	16.37	16.04	16.35
19	20.16	20.23	20.44	19.55	19.46	19.61	18.84	20.16
20	37.32	36.23	37.33	37.22	37.22	37.36	36.26	38.12
21	19.01	18.64	19.00	19.05	19.05	19.03	18.62	19.40
22	31.78	30.38	31.07	31.03	31.04	31.14	30.33	34.95
23	33.97	32.79	33.97	33.94	33.92	33.99	32.78	29.29
24	217.79	215.05	217.85	217.82	217.78	217.81	217.94	80.64
25	77.90	76.40	78.05	77.93	77.91	77.89	76.37	73.69
26	26.76	26.75	26.77	26.73	26.73	26.76	26.73	25.63
27	26.78	26.75	26.74	26.78	26.76	26.78	26.72	25.63
28	25.06	28.43	29.04	28.26	24.46	28.61	26.37	25.07
29	21.50	17.61	17.23	16.93	21.33	16.11	21.45	21.51
30	24.64	24.43	24.16	25.28	25.31	24.64	24.45	24.66
1′	171.63	171.14	180.34	172.52	171.55			171.68
2′	46.56	44.77	47.51	46.19	47.19			46.76
3′	70.90	n.d.	71.26	70.97	72.97			71.01
4′	27.56	26.7	27.98	27.86	27.68			27.59
5′	45.83	44.77	48.66	46.63	47.19			46.76
6′	171.63	171.14	172.6	173.22	172.80			171.68
7′	–	–	–	52.01	–	–	–	–
OAc-CH_3		21.13						
OAc-CO		171.84						

[a] Recorded in CD_3OD.
[b] Recorded in $CDCl_3$.

Compound **3**, called pholiol G, was isolated as a white amorphous solid with $[\alpha]_D^{25}$ +4 (*c* 0.1, MeOH). It gave the molecular formula $C_{36}H_{58}O_8$, which was determined *via* HRESIMS using the sodiated molecular ion peak at *m/z* 641.4017 $(M + Na)^+$ (calcd for $C_{36}H_{58}O_8Na$ 641.4029). In the comparison of the ^1H NMR spectra of **2** and **3**, the major differences were the remarkable paramagnetic shifts of H-3 (δ_H **2**: 4.79 d versus **3**: 3.20 d) and the absence of acetyl resonance (Table 1). To define the structure of **3**, a complete series of 2D NMR spectra was recorded and analyzed affording the structure 2*α*-(3-hydroxy-3-methylglutaroyloxy)-3*β*,25-dihydroxylanosta-8-en-24-one. Regarding the NOESY correlations between H-3/H_3-28, H-3/H-1b (δ_H 1.18 m), H-2/H-1a (δ_H 2.05 m), H-2/H_3-19, H-2/H_3-29, H-1$8_3$/H-20, and H-17/H_3-30, the stereochemistry of **3** was found to be the same as that of pholiol F (**2**). The fragmentation behaviour of **3** was investigated by direct-injection electrospray ionization quadrupole Orbitrap high-resolution mass spectrometry. The negative ion HRMS/MS spectrum with the proposed fragmentation pathway of **3** is shown in Fig. S56. Interestingly, mainly the 3-hydroxy-3-methylglutarate ester group of the precursor ion is involved in the fragmentation process and thus resulting in characteristic fragment ions.

Compound **4** was obtained as a white amorphous solid with optical rotation $[\alpha]_D^{25}$ +16.5 (*c* 0.5, MeOH). Its formula was assigned as $C_{37}H_{58}O_9$ by the protonated molecular ion at *m/z* 647.4166 $[M+H]^+$ (calcd for $C_{37}H_{59}O_9$, 647.4154) in HRESIMS. A detailed ^1H and ^{13}C J-MOD as well as 2D NMR spectroscopic analysis revealed that the difference between **3** and **4** was the replacement of the 7-methylene group in **3** for a keto group in **4** (δ_C 201.26). The position of the 7-keto group was established based on the HMBC correlations between C-7 and H_2-6 protons [δ_H 2.55 dd (16.3, 14.5 Hz), 2.36 m]. Furthermore, in the NMR spectra of **4**, an additional methoxy group could be observed [δ_H 3.68 s (3H), δ_C 52.01], which was assigned to the carboxymethyl ester of 3-hydroxy-3-methylglutarate moiety, as indicated by the HMBC correlation of OCH_3 group with C-6'. Therefore, compound **4** [lanosta-8-ene-3,25-diol-7,24-dione 2α-(methyl 3-hydroxy-3-methylglutarate)] was elucidated as depicted in Fig. 1 and named pholiol H.

Compound **5** with optical rotation $[\alpha]_D^{25}$ +11 (*c* 0.1, MeOH) had the molecular formula of $C_{36}H_{54}O_9$ as deduced from the prominent pseudomolecular ion peak in HRESIMS at *m/z* 631.3844 $[M+H]^+$ (calcd for $C_{36}H_{55}O_9$, 631.3841). The ^1H and ^{13}C NMR spectral data (Tables 1 and 2) depicted that **5** was also a lanostane-type triterpene, exhibiting a similar structure to that of pholiol E (**1**). A detailed comparison of these two compounds revealed an additional keto group at δ_C 200.27 in **5** instead of a methylene group, which is bonded at C-7 as displayed by the long-range correlation of C-7 with H-6. The tetrasubstituted $\Delta^{8,9}$ olefin was downfield shifted [δ_C **1**: 136.90 (C-8), 134.69 (C-9); **5**: 140.18 (C-8), 166.56 (C-9)] as a consequence of the emerging enone system (Yazdani et al., 2022). Diagnostic ^1H,^1H–COSY, HSQC, and HMBC correlations resulted in the assignment of all proton and carbon chemical shifts, and NOESY cross-peaks (Fig. 2) afforded the stereochemical assignment of compound **5** [2*α*-(3-hydroxy-3-methylglutaroyloxy)-25-hydroxylanosta-8-en-3,7,24-tri-one] named pholiol I.

The molecular formula of compound **6** was determined as $C_{30}H_{50}O_3$ by analyzing the prominent pseudomolecular ion peak at *m/z* 459.3833 $[M+H]^+$ (calcd for $C_{30}H_{51}O_3$ 459.3833) in HRESIMS. Compound **6** was

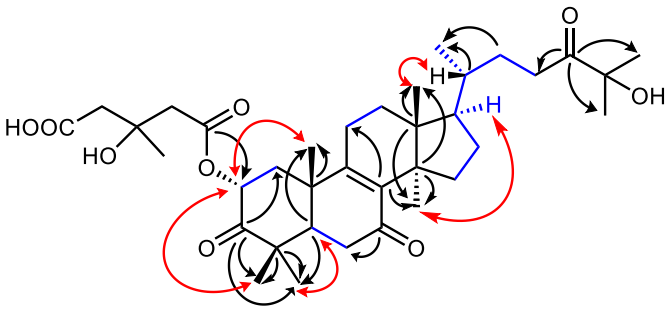

Fig. 2. Diagnostic $^{1}H,^{1}H$–COSY, HMBC and NOESY correlations of pholiol I (**5**).

obtained as a colorless amorphous solid with $[\alpha]_D^{25}$ +39 (*c* 0.1, MeOH). It exhibited close similarity to pholiol F (**2**), but the 3-hydroxy-3-methylglutarate ester moiety was absent in **6**. The 3-hydroxy, 8,9-olefin, 24-keto, and 25-hydroxy functionalities of lanostane triterpene were confirmed by the HMBC correlations of C-3 (δ_C 79.72) with H_3-28 (δ_H 0.98 s) and H_3-29 (δ_H 0.81 s); C-8 (δ_C 135.76) with H_3-30 (δ_H 0.92 s); C-9 (δ_C 136.09) with H_3-19 (δ_H 1.01 s) and H_2-7 (δ_H 2.07 m); C-24 (δ_C 217.81) with H_2-23 (δ_H 2.65 m); and C-25 (δ_C 77.89) with H_3-26 (δ_H 1.29 s) and H_3-27 (δ_H 1.29 s), respectively (Tables 1 and 2). Based on the Overhauser effects of H-3/H-5 and H-3/H_3-28 as well as the coupling constants of H-3 (10.1 and 6.3 Hz), the 3β orientation of the hydroxy group was determined [Nakamura et al., 2009]. Therefore, compound **6**, named pholiol J, was identified as 3β,25-dihydroxylanosta-8-en-24-one. This compound was first isolated from natural source, but previously synthesized without assignments of NMR chemical shifts (Yang et al., 2018). In their experiment, side-chain modified lanosterol derivatives were produced with the aim to develop compounds that reverse protein aggregation in cataracts. Lanosterol analogs with remarkable potency and efficacy in reversing several types of mutant crystalline aggregates were identified.

Compound **7**, named pholiol K, was isolated as a colorless amorphous solid with optical rotation $[\alpha]_D^{25}$ +29 (*c* 0.1, $CHCl_3$). Based on the HRESIMS pseudomolecular ion peak at *m/z* 457.3677 $[M+H]^+$ (calcd for $C_{30}H_{49}O_3$, 457.3676), the molecular formula of compound **7** was deduced to be $C_{30}H_{48}O_3$. The ^{13}C J-MOD spectrum of compound **7** demonstrated the existence of two keto groups (δ_C 215.13 and 217.94) in the molecule; one of them was placed at C-3 (δ_C 215.13) with regard to the HMBC correlations between C-3 and H_3-28 (δ_H 1.10 s), H_3-29 (δ_H 1.07 s), and H-2a (δ_H 2.57 m) whereas the other at C-24 (δ_C 217.94) based on the long-range correlations of C-24 and H_3-26 (δ_H 1.39 s), H_3-27 (δ_H 1.38 s), and H_2-23 (δ_H 2.55 m). The 25-hydroxy functionality was proposed by the carbon chemical shift value of $\delta_{C\text{-}25}$ 76.37. NOESY cross-peaks between H_3-18/H-20, H_3-28/H-5, and H-17/H_3-30 were consistent with the suggested structure of compound **7** [25-dihydroxylanosta-8-en-3,24-dione] (Fig. 1).

Compound **8** was identical in all of its spectral characteristics with (+)-clavaric acid. This compound was reported to be a specific inhibitor of human farnesyl protein transferase (FPTase) (IC_{50} 1.3 μM) (Lingham et al., 1998) and was first isolated from the fungus *Clavariadelphus truncatus* (Jayasuriya et al., 1998). The ^{1}H and ^{13}C NMR assignments of compound **8** were published in $CDCl_3$, but in our experiment, these data were determined in CD_3OD (Tables 1 and 2). The NOESY correlations between H-2/H_3-19, H-2/H_3-28, H_3-18/H-20, H-2/H-1a (δ_H 2.36), H-1a/H-11a (δ_H 2.16), and H-20/H-22a (δ_H 1.82) matched the relative stereostructure of (+)-clavaric acid.

2.2. Anti-inflammatory screening

The isolated compounds (**1**–**8**) and) pholiol C (**9**) were examined for their anti-inflammatory activity using COX-1, COX-2, 5-LOX, and 15-LOX assays, and Tables 3 and 4 present the results. The COX inhibitory activities of the compounds at 50 μM indicated a moderate-to-weak inhibition for the compounds. Dose–response investigations revealed that pholiols F (**2**) and (+)-clavaric acid (**8**) exhibited moderate anti-inflammatory activity on COX-2 with IC_{50} values of 439.8 and 766.7 μM, respectively. Furthermore, the other compounds had inhibition below 50% at the highest concentration tested (2.5 mM). Pholiols F (**2**), G (**3**), I (**5**), and C showed the best inhibitory activity against 5-LOX among the compounds (IC_{50} 194.5–519.7 μM). Pholiol F (**2**) with an IC_{50} value of 194.5 μM was the most active on 5-LOX test. However, all compounds were considered inactive against 15-LOX at the used concentrations.

Table 3
COX-1 and COX-2 inhibitory activities of the triterpenes of *P. populnea*.

Compound	COX-1			COX-2		
	Inhibitory (%)[a]	S.D.	IC_{50} (μM)	Inhibitory (%)	S.D.	IC_{50} (μM)
Pholiol E (**1**)	−10.42	9.43	–	7.00	4.59	–
Pholiol F (**2**)	20.32	0.19	–	35.74	10.67	439.8
Pholiol G (**3**)	−0.56	6.87	–	2.82	3.89	–
Pholiol H (**4**)	6.65	1.487	–	−2.50	4.99	–
Pholiol I (**5**)	4.89	17.26	–	−3.26	3.95	–
Pholiol J (**6**)	−16.16	13.84	–	−5.26	6.60	–
Pholiol K (**7**)	−37.13	3.20	–	−8.40	2.27	–
(+)-Clavaric acid (**8**)	20.96	9.99	–	37.27	8.54	766.7
Pholiol C (**9**)	17.7	0.64	–	3.28	36.76	–
Standard	50.94[b]	2.13	–	79.02	3.071	0.45[b]

[a] Relative percentage inhibition was assessed at 50 μM of the compounds and in triplicates. Dose–response investigations were conducted in duplicates with 2.5 mM as the highest concentration.
[b] Standards: SC560 for COX-1, Celecoxib for COX-2.

Table 4
5-LOX and 15-LOX inhibitory activities of the triterpenes of *P. populnea*.

Compound	5-LOX			15-LOX		
	Inhibitory (%)[a]	S.D.	IC_{50} (μM)	Inhibitory (%)	S.D.	IC_{50} (μM)
Pholiol E (**1**)	−35.25	3.05	–	−23.22	11.2	–
Pholiol F (**2**)	−7.91	16.28	194.5	−16.19	15.27	–
Pholiol G (**3**)	15.11	2.04	519.7	−77.38	24.05	–
Pholiol H (**4**)	−55.04	23.91	–	−94.87	11.21	–
Pholiol I (**5**)	0.72	4.07	480.5	−50.72	24.91	–
Pholiol J (**6**)	−102.2	19.33	–	−79.45	30.41	–
Pholiol K (**7**)	−302.5	8.65	–	−58.33	28.85	–
(+)-Clavaric acid (**8**)	−35.61	5.60	–	−39.6	22.47	–
Pholiol C (**9**)	17.27	9.16	370.1	−112.1	15.97	–
Standard	50.72	2.54	0.53[b]	103.5[b]	18.59	–

[a] Relative percentage inhibition was assessed at 100 μM of the compounds and in triplicates. Dose–response investigations were conducted in duplicates with 3 mM as the highest concentration.
[b] Standards: Zileuton for 5-LOX, NDGA for 15-LOX.

3. Conclusions

The present study showed a detailed mycochemical analysis of the chloroform and ethyl acetate extracts of the edible mushroom *P. populnea*. The combination of different chromatographic techniques and spectroscopic analysis resulted in the identification of eight lanostane triterpenoids (**1**–**8**), including the undescribed pholiols E–K (**1**–**7**). The evaluation of anti-inflammatory activity against cyclooxygenase (COX-1 and COX-2) and lipoxygenase (5-LOX and 15-LOX) enzymes revealed that pholiol F (**2**) and (+)-clavaric acid (**8**) bearing 2-(3-hydroxy-3-methylglutaryl) and only one keto group in their structure are the most effective COX-2 inhibitors, whereas the diester derivative pholiol F (**2**) possesses the best 5-LOX inhibitory activity. Pholiol F (**2**) with a dual 5-LOX/COX-2 inhibitory effect can be regarded as the most

interesting compound. It functions by blocking the formation of both prostaglandins and leukotrienes but does not influence lipoxin formation responsible for damaging the GI mucosa (Martel-Pelletier et al., 2003). In sum, our findings indicated that *P. populnea* is an excellent source of novel fungal metabolites.

4. Experimental

4.1. General

A Jasco P-2000 polarimeter was used to measure optical rotations (Jasco International, Co., Ltd., Hachioji, Tokyo, Japan). Molar Chemicals (Halásztelek, Hungary) and Sigma-Aldrich Kft. (Budapest, Hungary) supplied the chemicals used in this study. HPLC separations were conducted on a Shimadzu LC-10 A S HPLC instrument equipped with a UV–Vis detector (Shimadzu, Co., Ltd., KYOTO, Japan) over normal-phase (NP-HPLC, LiChrospher Si60, 5 μm, 250 × 4 mm) and reversed-phase (RP-HPLC, LiChrospher RP-18, 5 μm, 250 × 4 mm) columns. Furthermore, NP-HPLC was performed using a Zorbax-Sil column (250 × 9.4 mm, 5 μm; Agilent Technologies, Santa Clara, CA, USA) on a Waters HPLC instrument equipped with a PDA detector (Waters, Co., Ltd., Milford, USA). Flash chromatography (FC) was carried out on a CombiFlash Rf + Lumen instrument with integrated UV, UV–Vis, and ELS detection using reversed phase (RediSep C_{18} Bulk 950, Teledyne Isco, Lincoln, NE, USA) and normal phase (silica 60, 0.045–0.063 mm, Molar Chemicals, and RediSep Rf Gold, Teledyne Isco, Lincoln NE, USA) flash columns. Preparative thin-layer chromatography (TLC) was performed using silica plates (20 × 20 cm silica gel 60 F254, Merck 105,554). Sephadex LH-20 (25–100 μm, Sigma-Aldrich) was used for gel filtration. The direct-injection high-resolution mass spectrometry (HRMS) and high-resolution tandem mass spectrometry (HRMS/MS) measurements were performed by Waters Acquity I-Class UPLC™ (Milford, MA, UK) coupled to Thermo Scientific Q Exactive™ Plus Hybrid Quadrupole-Orbitrap™ (Waltham, MA, USA) mass spectrometer. The mass spectrometer was operated in heated electrospray ionization (ESI) mode with positive and negative ion detection. The instrument settings were as follows: capillary temperature 250 °C, S-Lens RF level 50, spray voltage 3.5 kV in positive and 2.5 kV in negative ionization mode. For HRMS/MS analysis, the collision energy was set to 30 eV, and 1 Da isolation window was applied. The eluent composition was 20/80/0.1 water/acetonitrile/formic acid (v/v/v) in positive ESI mode, while in negative ESI mode 20/80 water/acetonitrile was used (v/v). The flow rate was set to 0.4 mL/min. All samples were dissolved in methanol prior to the MS measurements. MassLynx 4.1 (Milford, MA, USA) software was used for UPLC and Xcalibur 4.3.73.11 software (Waltham, MA, USA) was used for spectra acquisition. NMR spectra were recorded in $CDCl_3$ or CD_3OD on a 500 MHz Bruker Avance DRX spectrometer (Bruker, Billerica, MA, USA) at 500 MHz (^{1}H) and 125 MHz (^{13}C). The signals of the deuterated solvents were taken as references. Two-dimensional NMR measurements were performed using the standard Bruker software. In the COSY, HSQC, and HMBC experiments, gradient-enhanced versions were used.

4.2. Mushroom material

Samples of *Pholiota populnea* (Pers.) Kuyper & Tjall.-Beuk. (Strophariaceae)were collected in the autumn of 2017 near Szeged, Hungary (46.400556, 20.190556), and identified by Attila Sándor (Mushroom Society of Szeged, Hungary). Fruiting bodies of *P. populnea* were stored at −20 °C until processing. A voucher specimen (No. H019) was deposited at the Department of Pharmacognosy, University of Szeged, Hungary.

4.3. Extraction and isolation

The fruiting bodies (4.2 kg) of *P. populnea* were ground in a blender and then percolated with MeOH (20 L) at room temperature. After evaporation of the solvent, the methanol extract (151 g) was dissolved in 50% aqueous MeOH and subjected to liquid–liquid partition using *n*-hexane (5 × 500 mL), chloroform (5 × 500 mL), and then ethyl acetate (5 × 500 mL). The ethyl acetate-soluble phase (16.7 g) was subjected to flash chromatography (NP-FC) on silica gel (80 g) using a gradient system of *n*-hexane–acetone (linear from 0% to 100% acetone, t = 60 min) and eluted with MeOH (100%, t = 5 min) at the end of this process, providing 17 combined fractions (E1–17). Fraction E7 (30 mg) was further separated by NP-HPLC (mobile phase: *n*-hexane–EtOAc–MeOH, 50:45:5), allowing the isolation of compound **6** (2.7 mg). Fraction E11 (4.2 g) was subjected to flash chromatography (NP-FC) on silica gel (40 g) using an *n*-hexane–acetone gradient system (linear from 0% to 100% acetone, t = 60 min) as a mobile phase, which also led to 14 fractions (EA 1–14). To further purify EA3 (370 mg), NP-HPLC was employed (mobile phase: cyclohexane–EtOAc 20:80) yielding fraction EA3-c (90 mg), which led to the isolation of **3** (2.4 mg), **5** (4.7 mg), **1** (25.8 mg), and **2** (3.7 mg) *via* RP-HPLC (mobile phase: H_2O–MeOH 20:80) separation. The chloroform-soluble phase (25.3 g) was subjected to NP-FC on silica gel (80 g) using a gradient system of *n*-hexane–EtOAc (linear from 40% to 100% EtOAc, t = 75 min) and eluted with MeOH (100%, t = 10 min) at the end of this process. Fractions with similar compositions were combined according to TLC monitoring (C1–C18). Compound **7** (2.1 mg) was produced by further purifying fraction C5 (390 mg) *via* NP-HPLC (mobile phase: *n*-hexane–EtOAc–MeOH 50:45:5). Fraction C7 (800 mg) was further separated using multiple steps of NP-FC, applying a gradient system of *n*-hexane–EtOAc (40 g of sorbent, linear elution from 45% to 100% EtOAc, t = 60 min) and cyclohexane–EtOAc (12 g of sorbent, linear from 0% to 100% EtOAc, t = 50 min), affording 14 (C7A a-n) and 12 (C7B a-l) combined fractions, respectively. Then, a final purification was conducted on C7Ae (17.5 mg) *via* preparative TLC using an *n*-hexane–EtOAc–MeOH (5:4:1) solvent system to produce compound **4** (2.5 mg). Finally, compound **8** (5.2 mg) was isolated from fraction C7Bb (5.9 mg) *via* RP-HPLC (mobile phase: H_2O–acetonitrile, 4:6).

4.3.1. Pholiol E (1)

White amorphous powder; $[\alpha]_D^{25}$ +49 (c 0.1, MeOH); ^{1}H and ^{13}C NMR data, see Tables 1 and 2; HRESIMS + m/z 617.4063 $[M+H]^+$ calcd for $C_{36}H_{57}O_8$ 617.4048; ESI– m/z 615.3926 $[M–H]^-$ (calcd for $C_{36}H_{55}O_8$ 615.3902).

4.3.2. Pholiol F (2)

White amorphous powder; $[\alpha]_D^{25}$ +5 (c 0.1, $CHCl_3$); ^{1}H and ^{13}C NMR data, see Tables 1 and 2; HRESIMS + m/z 661.4320 $[M+H]^+$ (calcd for $C_{38}H_{61}O_9$, 661.4310).

4.3.3. Pholiol G (3)

White amorphous solid; $[\alpha]_D^{25}$ +4 (c 0.1, MeOH); ^{1}H and ^{13}C NMR data, see Tables 1 and 2; HRESIMS + m/z 641.4017 $(M + Na)^+$ (calcd for $C_{36}H_{58}O_8Na$ 641.4029; HRESIMS– m/z 617.4089 $[M–H]^-$ (calcd for $C_{36}H_{57}O_8$, 617.4053).

4.3.4. Pholiol H (4)

White amorphous solid; $[\alpha]_D^{25}$ +16.5 (c 0.5, MeOH); ^{1}H and ^{13}C NMR data, see Tables 1 and 2; HRESIMS + m/z 647.4166 $[M+H]^+$ (calcd for $C_{37}H_{59}O_9$, 647.4154).

4.3.5. Pholiol I (5)

White amorphous powder; $[\alpha]_D^{25}$ +11 (*c* 0.1, MeOH); ^{1}H and ^{13}C NMR data, see Tables 1 and 2; HRESIMS + *m/z* 631.3844 $[M+H]^+$ (calcd for $C_{36}H_{55}O_9$, 631.3841).

4.3.6. Pholiol J (6)

Colorless amorphous solid; $[\alpha]_D^{25}$ +39 (c 0.1, MeOH); ^{1}H and ^{13}C NMR data, see Tables 1 and 2; HRESIMS + m/z 459.3833 $[M+H]^+$ (calcd for $C_{30}H_{51}O_3$ 459.3833)

4.3.7. Pholiol K (7)

Colorless amorphous solid; $[\alpha]_D^{25}$ +29 (c 0.1, $CHCl_3$), ^1H and ^{13}C NMR data, see Tables 1 and 2; HRESIMS + m/z 457.3677 $[M+H]^+$ (calcd for $C_{30}H_{49}O_3$, 457.3676).

4.3.7. (+)-Clavaric acid (8)

White amorphous powder; $[\alpha]_D$ +29 (*c* 0.1, MeOH); ^1H and ^{13}C NMR data, see Tables 1 and 2; HRESIMS– *m/z* 617.4086 $[M–H]^+$ (calcd for $C_{36}H_{57}O_8$, 617.4053).

4.4. Anti-inflammatory screening

4.4.1. Cyclooxygenase (COX) inhibitory activity

Based on the fluorometric method described in BioVision's COX-1 inhibitor screening kit leafkit (K548-100, BioVision, CA, USA) and COX-2 inhibitor screening kit leafkit (K547-100, BioVision, CA, USA), respectively, COX-1 and COX-2 inhibitory activities were assessed. The sample solutions were dissolved in DMSO and then in buffer to achieve suitable concentrations. In a 96-well white plate (655,101, F-bottom, Greiner Bio-One, Germany), 80-μL reaction mix (containing 76-μL assay buffer, 1-μL COX Probe, 2-μL COX cofactor, and 1-μL COX enzyme) was added to 10-μL sample solution, DMSO, and assay buffer to obtain test wells assigned for sample screen (S), negative control (N), and blank, respectively. Ten microliters of arachidonic/NaOH solution was added to each well using a multichannel pipette to start the reaction simultaneously, and the fluorescence of each well was measured kinetically at Ex/Em 550/610 nm, at 25 °C for 10 min, using a FluoStar Optima plate reader (BMG Labtech, Ortenberg, Germany). The COX inhibitory activity of SC560 and Celecoxib, standard inhibitors of COX-1 and COX-2, respectively, was also determined.

The change in fluorescence between two points, T_1 and T_2, were determined, and relative inhibition was computed as follows:

$$\text{Inhibition } \% = [(\text{change in N} - \text{change of S}) / \text{change in N}] \times 100$$

4.4.2. 5-Lipoxygenase (5-LOX) inhibitory activity

Based on the fluorometric method described in BioVision's 5-LOX inhibitor screening kit leafkit (K980-100, BioVision, CA, USA), measuring the decrease in fluorescence in the presence of potential 5-lipoxygenase inhibitors, 5-LOX inhibitory activity was tested. Briefly, to obtain a sample screen (S), the samples were dissolved in anhydrous DMSO, and 2-μL sample solutions were added to a 96-well white plate (655,101, F-bottom, Greiner Bio-One, Germany). Two microlitres each of assay buffer, anhydrous DMSO, and Zileuton solution, a standard inhibitor, were added to the corresponding wells to produce a blank, negative control (N), and positive control. Assay buffer (38 μL) was added to all wells and, subsequently, 40-μL reaction mix (containing 34-μL LOX assay buffer, 2-μL LOX probe, and 4-μL LOX enzyme). The reaction was started simultaneously after 10 min using a multichannel pipette to add 20-μL diluted substrate solution to each well, and the fluorescence of each well was determined kinetically at Ex/Em 485/520 nm, at 25 °C for 20 min, using a FluoStar Optima plate reader (BMG Labtech, Ortenberg, Germany).

The change in fluorescence between two points, T_1 (3 min) and T_2 (10 min), was determined, and relative inhibition was computed as follows:

$$\text{Inhibition } \% = [(\text{change in N} - \text{change in S}) / \text{change of N}] \times 100$$

4.4.3. 15-Lipoxygenase (15-LOX) inhibitory activity

15-LOX inhibitory activities of the compounds were assessed using Cayman's lipoxygenase inhibitor screening assay kit (760,700, Cayman Chemical, MI, USA), detecting and measuring the hydroperoxides produced in the lipoxygenation reaction using a lipoxygenase enzyme. Briefly, in a 96-well white plate (655,101, F-bottom, Greiner Bio-One, Germany), blank wells contained 100-μL assay buffer; negative-control wells contained 90-μL lipoxygenase standard solution and 10-μL assay buffer; standard inhibitor wells contained 90-μL lipoxygenase standard solution and 10-μL nordihydroguaiaretic acid (NDGA) solution, and sample wells contained 90-μL lipoxygenase standard solution and 10-μL sample solution prepared by dissolving in methanol and then assay buffer until suitable concentrations were achieved. After incubation for 10 min, 10-μL arachidonic/NaOH solution was added to all wells using a multichannel pipette to start the reaction simultaneously, and the plate was placed on a shaker. After 5 min, the reaction was stopped by adding 100 μL of chromogen to all wells, and the absorbance was read at 485 nm. The inhibition % was computed as

$$\text{inhibition } \% = [(\text{absorbance of control} - \text{absorbance of sample}) / \text{absorbance of control}] \times 100$$

The dose-effect investigations on the most active compounds were employed to measure the concentration, inhibiting 50% of COX-1, COX-2, 5-LOX, and 15-LOX enzyme activity. The sigmoidal dose–response model was obtained using GraphPad Prism 8.0 (La Jolla, CA, USA), and these were employed to determine the IC_{50} values of the compounds.

Declaration of competing interest

The authors declare that they have no known competing financial interests or personal relationships that could have appeared to influence the work reported in this paper.

Data availability

No data was used for the research described in the article.

Acknowledgments

This study was supported by National Research, Development and Innovation Office, Hungary (NKFIH; K135845). The authors are grateful to Attila Sándor for his help in the collection and identification of mushroom material.

Appendix A. Supplementary data

Supplementary data to this article can be found online at https://doi.org/10.1016/j.phytochem.2022.113480.

References

Aichour, S., Haba, H., Benkhaled, M., Harakat, D., Lavaud, C., 2014. Terpenoids and other constituents from *Euphorbia bupleuroides*. Phytochem. Lett. 10, 198–203.

Bao, T.R.G., Long, G.Q., Wang, Y., Wang, Q., Liu, X.L., Hu, G.S., Gao, X.X., Wang, A.H., Jia, J.M., 2019. New lanostane-type triterpenes with anti-inflammatory Activity from the epidermis of *Wolfiporia cocos*. Molecules 24, 1888.

Chen, H.-P., Zhao, Z.-Z., Li, Z.-H., Huang, Y., Zhang, S.-B., Tang, Y., Yao, J.-N., Chen, L., Isaka, M., Feng, T., Liu, J.-K., 2018. Anti-proliferative and anti-inflammatory lanostane triterpenoids from the Polish edible mushroom *Macrolepiota procera*. J. Agric. Food Chem. 66, 3146–3154.

Hu, Z., Du, R., Xiu, L., Bian, Z., Ma, C., Sato, N., Hattori, M., Zhang, H., Liang, Y., Yu, S., Wang, X., 2020. Protective effect of triterpenes of *Ganoderma lucidum* on

lipopolysaccharide-induced inflammatory responses and acute liver injury. Cytokine 127, 154917.
Jayasuriya, H., Silverman, K.C., Zink, D.L., Jenkins, R.G., Sanchez, M., Pelaez, F., Vilella, D., Lingham, R.B., Singh, S.B., 1998. Clavaric acid: a triterpenoid inhibitor of farnesyl-protein transferase from. Clavariadelphus truncates. J. Nat. Prod. 61, 1568–1570.
Lingham, R.B., Silverman, K.C., Jayasuriya, H., Kim, B.M., Amo, S.E., Wilson, F.R., Rew, D.J., Schaber, M.D., Bergstrom, J.D., Koblan, K.S., Graham, S.L., Kohl, N.E., Gibbs, J.B., Singh, S.B., 1998. Clavaric acid and steroidal analogues as RAS- and FPP-directed inhibitors of human farnesyl-protein transferase. J. Med. Chem. 41, 4492–4501.
Martel-Pelletier, J., Lajeunesse, D., Reboul, P., Pelletier, J.-P., 2003. Therapeutic role of dual inhibitors of 5-LOX and COX, selective and non-selective non-steroidal anti-inflammatory drugs. Ann. Rheum. Dis. 62, 501–509. https://doi.org/10.1136/ard.62.6.501.
Nakamura, S., Iwami, J., Matsuda, H., Mizuno, S., Yoshikawa, M., 2009. Absolute stereostructures of inoterpenes A–F from sclerotia of *Inonotus obliquus*. Tetrahedron 65, 2443–2450.
Öztürk, M., Tel-Çayan, G., Muhammad, A., Terzioğlu, P., Duru, M.E., 2015. Mushrooms: a source of exciting bioactive compounds. Stud. Nat. Prod. Chem. Chapter 10 (45), 363–456.
Ványolós, A., Muszyńska, B., Chuluunbaatar, B., Gdula-Argasińska, J., Kała, K., Hohmann, J., 2020. Extracts and steroids from the edible mushroom *Hypholoma lateritium* exhibit anti-inflammatory properties by inhibition of COX-2 and activation of Nrf2. Chem. Biodivers. 17, e2000391.
Yang, X., Chen, X.J., Yang, Z., Xi, Y.-B., Wang, L., Wu, Y., Yan, Y.-B., Rao, Y., 2018. Synthesis, evaluation, and structure-activity relationship study of lanosterol derivatives to reverse mutant-crystallin-induced protein aggregation. J. Med. Chem. 61, 8693–8706. https://doi.org/10.1021/acs.jmedchem.8b00705.
Yazdani, M., Béni, Z., Dékány, M., Szemerédi, N., Spengler, G., Hohmann, J., Ványolós, A., 2022. Triterpenes from *Pholiota populnea* as cytotoxic agents and chemosensitizers to overcome multidrug resistance of cancer cells. J. Nat. Prod. 85, 910–916.
Zhang, F.-L., Shi, C., Sun, L.-T., Yang, H.-X., He, J., Li, Z.-H., Feng, T., Liu, J.-K., 2021. Chemical constituents and their biological activities from the mushroom *Pyropolyporus fomentarius*. Phytochemistry 183, 112625.